Nanoscale spatial organization of the *HoxD* gene cluster in distinct transcriptional states

Pierre J. Fabre[a], Alexander Benke[b], Elisabeth Joye[a], Thi Hanh Nguyen Huynh[c], Suliana Manley[b,1], and Denis Duboule[a,c,1]

[a]School of Life Sciences, Ecole Polytechnique Fédérale de Lausanne, 1015 Lausanne, Switzerland; [b]Laboratory of Experimental Biophysics, Ecole Polytechnique Fédérale de Lausanne, 1015 Lausanne, Switzerland; and [c]Department of Genetics and Evolution, University of Geneva, 1211 Geneva 4, Switzerland

Contributed by Denis Duboule, September 14, 2015 (sent for review July 21, 2015; reviewed by Victor Corces and Luca Giorgetti)

Chromatin condensation plays an important role in the regulation of gene expression. Recently, it was shown that the transcriptional activation of *Hoxd* genes during vertebrate digit development involves modifications in 3D interactions within and around the *HoxD* gene cluster. This reorganization follows a global transition from one set of regulatory contacts to another, between two topologically associating domains (TADs) located on either side of the *HoxD* locus. Here, we use 3D DNA FISH to assess the spatial organization of chromatin at and around the *HoxD* gene cluster and report that although the two TADs are tightly associated, they appear as spatially distinct units. We measured the relative position of genes within the cluster and found that they segregate over long distances, suggesting that a physical elongation of the *HoxD* cluster can occur. We analyzed this possibility by super-resolution imaging (STORM) and found that tissues with distinct transcriptional activity exhibit differing degrees of elongation. We also observed that the morphological change of the *HoxD* cluster in developing digits is associated with its position at the boundary between the two TADs. Such variations in the fine-scale architecture of the gene cluster suggest causal links among its spatial configuration, transcriptional activation, and the flanking chromatin context.

DNA FISH | super-resolution microscopy | limb development | topologically associating domains | *HoxD*

In the nuclei of mammalian cells, chromatin is packaged according to several levels of organization (1–3), which can either reflect or affect transcriptional regulation (e.g., ref. 4). By combining DNA FISH and microscopy, it was shown that chromatin decondensation occurs concomitantly with transcriptional activation (5), suggesting that the opening of chromatin makes gene promoters accessible for transcription. Recently, however, studies involving super-resolution microscopy have revealed a more complex relationship, showing that a higher compaction of chromatin can also be associated with an active state of transcription (6). In this latter case, the compaction of local regulatory elements allowed for a stronger enhancer effect, leading to a more robust activation.

Approaches based on chromosome conformation capture [and derivatives thereof (7)] at the mammalian *HoxD* locus have revealed that interactions between genes and their enhancers can occur not only during an active phase of transcription but also in the absence of transcriptional read out, in cells that do not necessarily express the related target genes (8). Such constitutive contacts covering large regulatory landscapes and their target gene or genes were found to be present in mammals genome-wide (9) and are referred to as topologically associating domains, or TADs (9, 10). TADs have been associated with a variety of regulatory functions (11), either in their implementation (e.g., ref. 12) or in their emergence during vertebrate evolution (13, 14).

Hox gene clusters have been successfully used to study the functional organization of TADs (15–17), as well as the relationship between the progressive decompaction of both genes and enhancers and their transcriptional read-out. Studies of the mouse *HoxD* cluster have provided insights into the global regulation of its nine consecutive genes during limb development, including the presence of multiple regulatory sequences spanning a 2-megabase large DNA interval (18). Recently, this gene cluster, similar to its *HoxA* relative (14, 15), was shown to reside at a boundary between two TADs (located ca. between *Hoxd11* and *Hoxd12*), with each TAD containing enhancers required to regulate different subgroups of genes in developing organs or structures (9, 16, 19) such as distal limbs, proximal limbs, genitals, or the cecum. Interestingly, all enhancers sharing a particular specificity are found within the same TAD, and thus far, no cell type or tissue was reported where these two opposite regulatory landscapes would operate concomitantly (8, 16, 17, 19), suggesting a functional switch occurs between these two TADs in their capacity to regulate subsets of target *Hoxd* genes.

TADs were originally defined by biochemical approaches (9, 10). The correspondence between the averaging of multiple interactions, some of them of unknown significance, on the one hand (see ref. 20), and a chromatin structure in the nuclear space of single cells, on the other hand, is of great interest and has recently come under discussion (see ref. 21). In this study, we used DNA FISH to show that the two TADs splitting the *HoxD* locus are distinct chromatin units, which rarely overlap despite their close association in space. Within this well-defined 3D organization, *Hoxd* genes can segregate over large distances. By using super-resolution microscopy, we observe that these large distances result from extensive elongation events over relatively short genomic distances, which appear to be maximal in tissue with high levels of *Hoxd* gene transcription. Our data suggest this elongation of the *HoxD* cluster is facilitated by its genomic position at the boundary between two TADs.

Significance

Ultrastructural chromatin dynamics may play a key role in regulating transcriptional activation. Here we have used super-resolution microscopy to study the folding mechanics of the *HoxD* cluster, as assayed by following the elongation of chromatin in single cells with different status of *Hox* gene activation. We observed that the spatial separation of *Hoxd* genes is strongest in those tissues where they are highly expressed. We also document that the opening of chromatin precedes transcription and that the strongest elongations are observed at the location of the boundary between two major topologically associating domains (TADs). These results shed light on how spatial compartmentalization is achieved, likely to accompany efficient chromatin reorganization upon activation of transcriptional switches.

Author contributions: P.J.F., S.M., and D.D. designed research; P.J.F., A.B., E.J., and T.H.N.H. performed research; S.M. and D.D. contributed new reagents/analytic tools; P.J.F., A.B., E.J., and S.M. analyzed data; and P.J.F., A.B., S.M., and D.D. wrote the paper.

Reviewers: V.C., Emory University; and L.G., Friedrich Miescher Institute for Biomedical Research.

The authors declare no conflict of interest.

Freely available online through the PNAS open access option.

Data deposition: The RNA-seq data reported in this paper have been deposited in the Gene Expression Omnibus (GEO) database, www.ncbi.nlm.nih.gov/geo (accession no. GSE72285).

[1]To whom correspondence may be addressed. Email: Denis.Duboule@epfl.ch or suliana.manley@epfl.ch.

This article contains supporting information online at www.pnas.org/lookup/suppl/doi:10.1073/pnas.1517972112/-/DCSupplemental.

Results

***Hoxd* Genes Are Localized at the Boundary Between Two TADs.** To directly observe the chromatin topology surrounding the *HoxD* cluster, we used 3D DNA FISH by labeling several consecutive BACs per TAD, such as to cover each TAD with a different color (Fig. 1*A* and *SI Appendix*, Table S1), and thus to assess the general chromatin spatial organization surrounding *HoxD* (Fig. 1*B*). In both active (forelimb) and inactive (forebrain) cells, we observed that TADs are organized as two dense and distinct units, closely associated in the nuclear space (Fig. 1*C*). High-resolution images using structured illumination microscopy showed that the TADs did not intermingle, and rarely overlapped in any substantial manner (Fig. 1*D*). This segregation was much less pronounced when BAC probes belonging to the same TAD were used as controls (*SI Appendix*, Fig. S1).

We measured the distance between TAD centers, which ranged from 0.20 to 1.40 μm, with an average of about 0.79 μm ($n > 1{,}000$ pairs). Because previous studies using chromosome conformation capture (4C) had revealed a dynamic switch in contacts between *Hoxd* genes and the two TADs in the proximal versus distal parts of developing forelimbs (16), we assessed whether this inter-TAD distance would change between these distinct limb domains, but found no significant difference (Fig. 1 *B*, *C*, and *E*). A detailed analysis of chromatin morphology revealed that the TADs are rather compact, with low ellipticity (Fig. 1*F*). We nevertheless observed a slight variation in ellipticity in cellular domains displaying different *Hoxd* gene expression patterns. Both TADs indeed appeared slightly less elongated in presumptive digit cells in the distal part of the limb (Fig. 1*F*), yet their global structure was rather stable in all analyzed situations. Finally, we assessed the position of the *HoxD* cluster relative to the TADs, using a 39-kb large fosmid probe covering the *Hoxd8* to *Hoxd12* genes. As expected, the signal was consistently detected at the interface between the two chromatin domains (Fig. 1*G*). In some cases, the *HoxD* cluster signal appeared somewhat elongated (arrowheads, Fig. 1*G*).

***Hoxd* Genes Are Close to Their Regulatory Islands.** The fact that TADs display comparably condensed aspects in both proximal and distal limb cells in vivo, that is, independent from their transcriptional activities, supports the view of a preformed or poised "background regulatory structure" (8); that is, a state of preferential chromatin compaction within a given TAD in which constitutive interactions occur without necessarily eliciting a transcriptional output (9, 11). In a previous study using FISH in ES cells, the *Hoxd1* gene localized at a substantial distance from *Hoxd13,* suggesting that the *HoxD* cluster could display spatially distinct moieties with its centromeric region (containing *Hoxd13*) positioned at the TAD boundary (22). To assess whether this apparent decompaction of *Hoxd* genes is linked to their relative topological position within the cluster and, consequently, whether their inclusion into either one of the TADs or their location at the inter-TADs boundary could explain this tendency to decompact, we examined the spatial relationships between four different parts of the *HoxD* cluster.

We used fosmid clones either covering the *Hoxd1* gene or the *Hoxd3* to *Hoxd4* region, (i.e., two regions normally included within the telomeric TAD), covering the *Hoxd13* gene, and hence entirely positioned within the centromeric TAD, or covering the *Hoxd8* to *Hoxd12* region located at or around the inter-TAD boundary (16) (Fig. 1*H*). We measured the distances between combinations of two probes and found that parts of the *HoxD* cluster could be separated from one another by more than 500 nm (Fig. 1 *I*–*K*). Of note, the distances measured between the centers of both signals generally correlate with the genomic distance (Fig. 1*J* and *SI Appendix*, Table S2). In this respect, we noticed that the telomeric extremity of the *HoxD* cluster, as monitored by the *Hoxd1* probe, was clearly separated from the main part of the cluster, with an average distance between *Hoxd1* and *Hoxd11* or *Hoxd13* of more than 700 nm (Fig. 1*J*). This apparent separation between *Hoxd1* and the rest of the cluster was, however, not constant and followed a broad distribution (Fig. 1*K*).

Super-Resolution Microscopy of the *HoxD* Locus. This spatial separation between different parts of the *HoxD* cluster is reminiscent of a model in which groups of active and inactive genes within *HoxD* form physically distinct and highly dynamic subdomains (23). To more directly examine the conformation of the *HoxD* cluster in single cells, we labeled its entire genomic sequence by using a 160-kb large BAC as a DNA probe and carried out DNA FISH. The morphology of the *HoxD* cluster was subsequently resolved using stochastic optical reconstruction microscopy (STORM), a type of super-resolution imaging based on sequential imaging of single-molecule signals (24–26). As a control, we used a probe of similar size located nearby, within the telomeric gene desert (Fig. 2*A*).

We initially examined sections of embryonic brain where the *HoxD* cluster is transcriptionally silent. Both the control and *HoxD* probes appeared as compact objects (Fig. 2 *B* and *E*). However, cells from the developing distal forelimb; that is, a tissue with robust transcription of at least the *Hoxd13* to *Hoxd9* genes (27) (Fig. 3), displayed a higher diversity of morphologies (Fig. 2 *C* and *F*). Although the total area of the object appeared unchanged, the signal detected in many cells of the forelimb tissues was substantially more elongated (*SI Appendix*, Fig. S2). We quantified this variation in elongation by the aspect ratio and the circularity of the objects. The major axis of the cluster divided by its minor axis (aspect ratio) was significantly higher in active forelimb cells than in inactive forebrain cells (Fig. 2*H*), where circularity was also lower (Fig. 2*I*).

As elongation was maximal in limb cells displaying a high level of *Hoxd* transcription, we assessed whether transcription could cause elongation by evaluating the cluster morphology in ES cells, a cell type in which *Hoxd* genes have not yet been activated and are labeled by positive and negative chromatin marks, potentially reflective of a poised transcriptional state (28). In these cells, many alleles showed an elongated aspect, with a circularity index close to that scored in forelimb cells, and thus significantly different from the data obtained in brain cells (Fig. 2 *D*, *G*, and *I*). From this observation, we conclude that the elongation observed by using STORM microscopy seems to be an important feature of an "open" *HoxD* cluster, observed either in ES cells where the cluster is poised to be transcribed or in cells where transcription indeed occurs. Finally, we measured the extent of the elongated structure and found that the signals can span more than 500 nm. This high extension rate is consistent with our previous measurements (Fig. 1*J*) and is in the range predicted by mathematical modeling (29).

Chromatin Elongation at Super Resolution. The mechanisms underlying such an elongation process are unclear. Opening and/or relaxation of chromatin may be a consequence of active transcription driven by elongating RNA polymerase II and consequent chromatin remodeling. Alternatively, changes in chromatin morphology could result from states of histone modifications not necessarily associated with different transcriptional activities. For example, in both brain and ES cells, the *HoxD* cluster is covered by polycomb-associated chromatin marks such as H3K27me3, which may participate in its compaction via the recruitment of the PRC1 complex (22, 28, 30). However, the H3K27me3 coverage observed over *HoxD* in ES cells is significantly weaker than in brain cells (23), which may be related to the presence of H3K4me3 marks in the former sample. Accordingly, a poised chromatin state may show a level of decompaction comparable to that of transcriptionally active chromatin.

We investigated this issue by using super-resolution microscopy with four smaller DNA probes spanning different subregions of the *HoxD* cluster (Fig. 1*H*, enlarged in Fig. 3*A*). These subregions displayed differential coverage by polycomb-associated marks in either distal or proximal limb bud cells (16), and thus were used to evaluate a potential link between the elongation

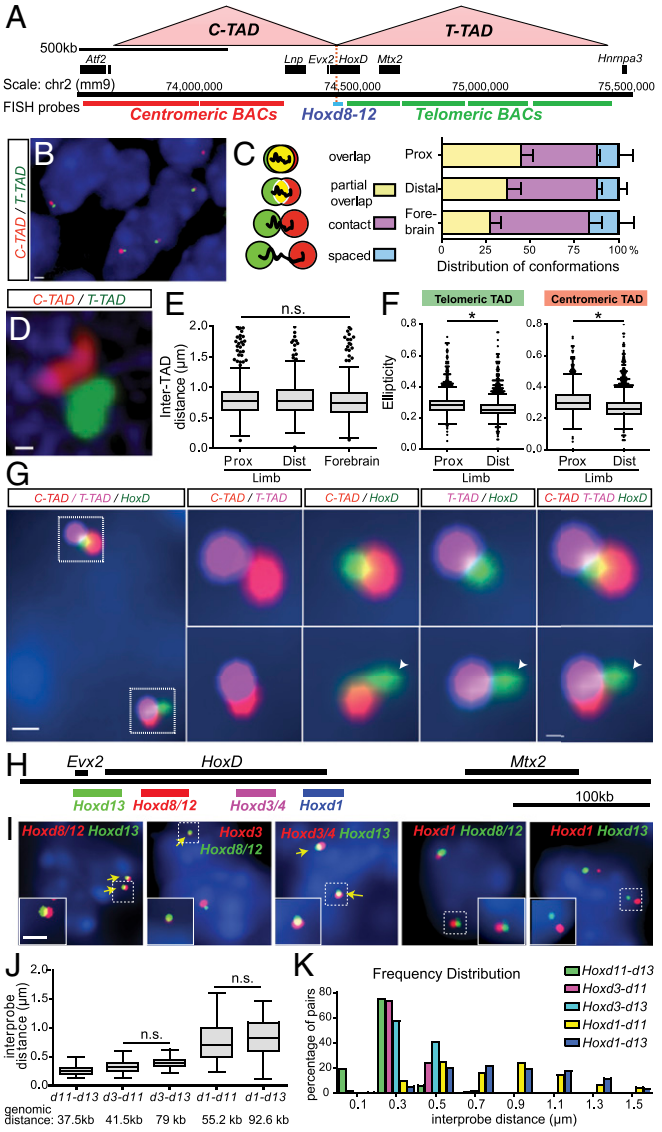

Fig. 1. The *HoxD* cluster is at the interface between two TADs. (*A*) Schematic of the centromeric and telomeric TADs (C-TAD; T-TAD) using public data available under ref. 9 with genes as black boxes below and the relative localization of the probes (in red, blue and green) used in the DNA FISH experiments. The red dotted line represents the TAD boundary within *HoxD*. (*B*) E12.5 distal forelimb nuclei stained with DAPI (blue) and the centromeric (red) and telomeric (green) TADs. (Scale bar, 1 μm.) (*C*) Schematic (*Left*) and distributions (*Right*) of the various configurations observed by FISH in *B*. Prox and Dist, proximal and distal limb cells, respectively. (*D*) An example of structured illumination microscopy showing the absence of overlap between the two TADs. (Scale bar, 500 nm.) (*E* and *F*) Quantifications of the parameters observed under *B*. (*E*) Distances between the centers of both TADs. n.s., nonsignificant, using a Kruskall-Wallis test followed by Dunn's multiple comparison posttest. (*F*) Ellipticity measured for both the telomeric (*left*) and centromeric (*right*). *$P < 0.0001$, using unpaired *t* tests. (*G*) Position of the *HoxD* cluster for two alleles of a representative distal forelimb cell, using a fosmid probe specific for the genes *Hoxd8* to *Hoxd12* (green). The signal is scored between the centromeric (red) and telomeric (magenta) TADs. (Scale bar, 500 nm.) (*Right*) Close-ups of both alleles with white arrowheads showing an elongated *HoxD* cluster. (Scale bar, 200 nm.) (*H–K*) Distances between various probes localized within the *HoxD* cluster (*H*). (*I*) Forelimb cells nuclei stained with DAPI (blue) and DNA FISH (red and green) for different combinations of *Hoxd* fosmids (*Top*). (Scale bar, 500 nm.) (*J*) Quantification of the distribution of interprobe distances between selected pairs of probes. The statistical significance between datasets was tested using using Kruskall-Wallis test followed by Dunn's multiple comparison posttest. All were significantly different ($P < 0.05$) except the ones indicated with n.s. See *SI Appendix*, Table S2 for details. (*K*) Frequency distribution of the measurements shown in *J*.

of the cluster and either its transcriptional activity or the presence of polycomb-associated proteins. For instance, the probe containing *Hoxd1* is covered by H3K27me3 marks in distal cells, whereas the *Hoxd8* to *Hoxd12* fragment shows a moderate coverage. In contrast, the probes encompassing either the *Hoxd11* to *Hoxd13* or the *Hoxd13* to *Evx2* DNA intervals are free of H3K27me3 in embryonic day (E) 12.5 distal and active cells, likely as a consequence of high transcriptional activity (Fig. 3*A*).

Each fosmid clone was labeled with the same Alexa 647 fluorophore and its signal analyzed by STORM microscopy. By comparing the signal morphologies (Fig. 3*B*), we noticed that the *Hoxd1* signals did not appear significantly more compact than the others (Fig. 3*B*; representative examples). If anything, this area of the *HoxD* cluster, which is densely covered by H3K27me3 marks, was slightly less circular than images obtained from the fosmids covering regions with lower amounts of H3K27me3 and highly expressed genes (Fig. 3*C*). To complement this observation, we labeled the two fosmid clones containing either the *Hoxd1* or the *Hoxd8* to *Hoxd12* regions, using Alexa 647 and Alexa 555, respectively, to directly assess their relative morphologies within the same cells. These experiments confirmed that these two DNA regions were decompacted to similar extents in the same cells (*SI Appendix*, Fig. S2*B*). The most extensive elongation observed (*Hoxd8-d12,* Fig. 3 *B* and *C*) matches the set of genes that was shown to have cell-specific long-range DNA contacts in the developing forelimb (16). To test whether decompaction could change with a modification of long-range contacts, we compared the two tissues in which the pattern of long-range interactions differs drastically: the proximal and distal forelimbs (Fig. 3*D*). Here we observed similar structures, both of them significantly more dispersed than that which was observed in the forebrain, used as a negative control (Fig. 3*D*).

We next investigated whether such a decompaction would also be observed in another tissue in which the *HoxD* cluster is strongly activated, and thus imaged the *Hoxd8-d12* region in the developing trunk. We compared forebrain cells in which the cluster is completely inactive, anterior trunk cells in which transcription occurs from *Hoxd1* to *Hoxd8* only, and posterior trunk cells in which *Hoxd1* to *Hoxd12* are activated. We observed the strongest decompaction in those tissue with the highest level of transcription (Fig. 3*E*), suggesting the existence of a link between transcription and the unfolded structure of *Hox* genes.

Effect of the Gene Deserts on Compaction. 4C studies using microdissected limb samples have indicated that parts of the *HoxD* cluster are strongly contacted by enhancer sequences located in both the centromeric and telomeric TADs (8, 16). Such strong enhancer contacts may exert forces upon the *HoxD* cluster, leading to variations in its global chromatin architecture. We assessed this possibility by analyzing three genetic perturbations in which *Hoxd* genes were separated from their respective enhancers by large targeted inversions (31, 32). The first allele was an inversion separating *HoxD* from its telomeric TAD by displacing the latter by 28 Mb *(Inv(attP-cd44*; Fig. 3*F*), which switched off *Hoxd9-11* in proximal limb cells and decreased their transcription in distal limb cells. The morphologies of signals detected when using this large inversion were as elongated as in noninverted cells, showing that the immediate regulatory neighborhood, even though it contains sequences interacting with the probe, was not critical in the shaping of the cluster, at least in these particular conditions. In both the inverted and wild-type loci, a low circularity index was determined for the *Hoxd8* to *Hoxd12* DNA region (Fig. 3 *G* and *H*), suggesting that the presence of genuine enhancer sequences and constitutive interactions (16) is not necessary for the decompaction of the *HoxD* cluster.

We also assessed the *Inv*(*Nsi-Itga6*) centromeric inversion (*SI Appendix*, Fig. S3 *A* and *B*), which repositions the centromeric regulatory sequences several Mb away from the cluster, thus abrogating all specific enhancer–promoter interactions occurring during digit development and, consequently, turning off *Hoxd*

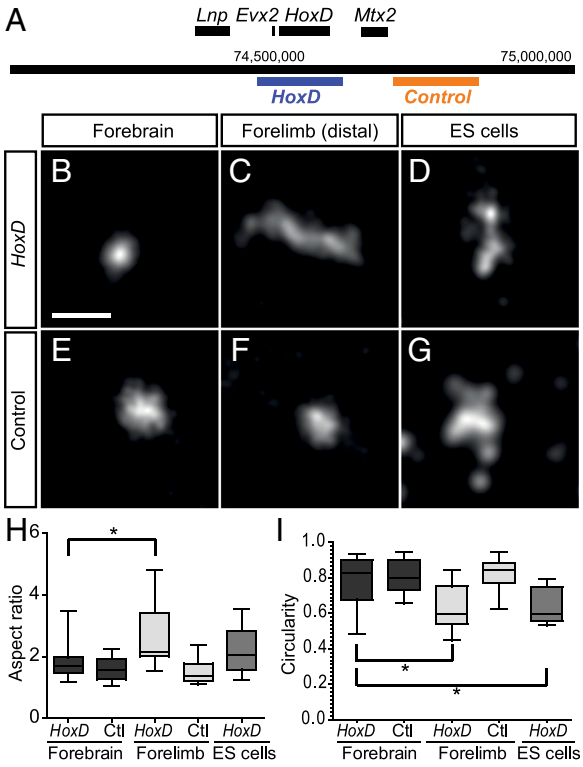

Fig. 2. Distinct conformations of the *HoxD* cluster visible by STORM microscopy. (*A*) Schematic view of the two BAC clones, 160 and 175 kb large, respectively, used to visualize the *HoxD* cluster and part of the telomeric gene desert, using STORM imaging. (*B*–*G*) DNA FISH using Alexa 647 and resolved through STORM, using either "inactive" forebrain (*B* and *E*), "active" distal forelimb (*C* and *F*), or synchronized ES (*D* and *G*) cells. (Scale bar, 200 nm.) (*H* and *I*) For the same cells, quantifications of aspect ratio (*H*) and circularity (*I*) are shown, where the asterisk indicates $P < 0.01$, using a Kruskall-Wallis test followed by Dunn's multiple comparison posttest (see *SI Appendix, Materials and Methods*).

genes transcription (33). Again, the decompacted aspect of the *HoxD* cluster was not dramatically modified after STORM imaging (*SI Appendix*, Fig. S3*B*). Finally, we used a large inversion, with a breakpoint located between *Hoxd10* and *Hoxd11*, thus splitting the *HoxD* cluster into two parts, leaving in place only from *Hoxd11* to *Hoxd13* and their centromeric gene desert (ref. 31; scheme in *SI Appendix*, Fig. S3). We monitored the aspect ratio of the short remaining cluster, using the fosmid probe covering from *Hoxd11* to *Hoxd13*, and found no difference in elongation (*SI Appendix*, Fig. S3*C*), suggesting a full *HoxD* cluster is not critical to spatially organizing chromatin in its various parts.

Discussion

The organization of chromatin in the nuclear space is a critical parameter for the proper control of transcription, and the extent of chromatin elongation at a given genetic locus may reflect its capacity to be efficiently transcribed (34). We previously determined that the *HoxD* gene cluster was the target of a bimodal type of global regulation, exerted from either the telomeric or centromeric gene deserts, two regulatory landscapes matching TADs, and separated by the *HoxD* cluster itself (9, 16). However, chromosome conformation capture-based experiments average the treatment of several million independent cells, and the presence of dense and compact chromatin architectures flanking the *HoxD* cluster remained to be shown at the cellular level. Here, by concomitantly labeling series of BACs spanning specifically the two TADs, we demonstrate that such configurations indeed exist as dense and separate objects in individual cells, as previously seen on a specific locus at the X-chromosome (10), with a low level of partial overlap consistent with the reduced number of interactions observed in 4C between the two TADs (16, 17). This observation was confirmed by structured illumination microscopy. The distances between TADs were comparable between cells, whether or not they expressed *Hoxd* genes, supporting the existence of a poised regulatory structure already present in the absence of transcription (8). However, the direct visualization of TADs at this locus is not informative regarding potential fluctuations in contacts within each TAD, from one cell to another (20). It nevertheless demonstrates that such dense structures exist in all cells and on both alleles.

By using super-resolution microscopy (STORM), we scored the most extensively elongated forms in cells from either the developing distal forelimb or the posterior trunk, two tissues in which several *Hoxd* genes are strongly active. In contrast, dense and compact structures were scored either in brain cells, negative for all *Hox* gene transcription at this stage, or when using a control probe located outside the gene cluster. These elongated morphologies generally occurred along a major axis and appeared continuous, either when using large probes covering the whole cluster or with smaller probes detecting only one or a few genes. In distal forelimb cells, however, where the *Hoxd1* to *Hoxd4* region is covered by H3K27me3 chromatin marks (16), we did not observe any significant asymmetric compaction. In contrast, the inactive part of the *HoxD* cluster was at least as elongated as the transcriptionally active region. One explanation for this unexpected observation may be the robust and nonproductive contacts established by *Hoxd1* with the telomeric TAD (16), which may lead to tensions elongating the gene cluster (see following).

A significant elongation of the gene cluster was also scored in ES cells, even though the entire *HoxD* cluster is labeled with both H3K4me3 and H3K27me3 chromatin marks (22, 28, 30) associated with the formation of local chromatin domains (23, 35), in contrast with the idea that *Hox* clusters adopt a "closed" conformation whenever genes are silent (23). In ES cells, however, the 4C interaction patterns are much weaker than in brain cells (35), probably because of the presence of bivalent chromatin marks and the concomitant reduced amount of H3K27me3 modifications [Fig. 1 and figure S1 in ref. 35, the latter being even weaker when ES cells were cultured in 2i medium (36)]. It was also noticed that *Hoxd* genes established many more interactions with the neighboring gene deserts in ES cells than in brain cells (35), where most interactions involved the gene cluster itself, further suggesting a more decompacted configuration of the locus in ES cells. Therefore, the vast majority of ES cells may display decompacted chromatin at their *Hox* loci. The presence of some H3K27me3-labeled nucleosomes may induce enough transitory interactions to be translated into read counts after deep sequencing of 4C products.

Altogether, these data suggest that in the developing limbs, the *HoxD* cluster is decompacted, with an elongated shape including both active and inactive genes. Therefore, the coverage of specific parts of the cluster by polycomb complexes, depending on the proximal versus distal position of the cells (8, 16) and observed in other functional contexts (30, 37, 38), does not seem to significantly influence its level of compaction. The distances apparently associated with these elongated forms correspond to previous distance predictions established by mathematical modeling (29). Stretching events associated with transcription were also reported, which seem to occur within this range of elongation lengths (5), and several recent studies either describe or predict distances ranging from 300 to more than 1,000 nm (39, 40). The elongation of the *HoxD* cluster in limb cells despite its partial labeling by H3K27me3 may reflect an influence from the flanking TADs in extending the structure in both directions, following either productive or constitutive interactions. We evaluated this possibility by using three large inversions modifying the global relationships between the gene cluster and its two regulatory landscapes. However, none of these rearrangements did affect the capacity of the cluster to elongate. If anything, elongation

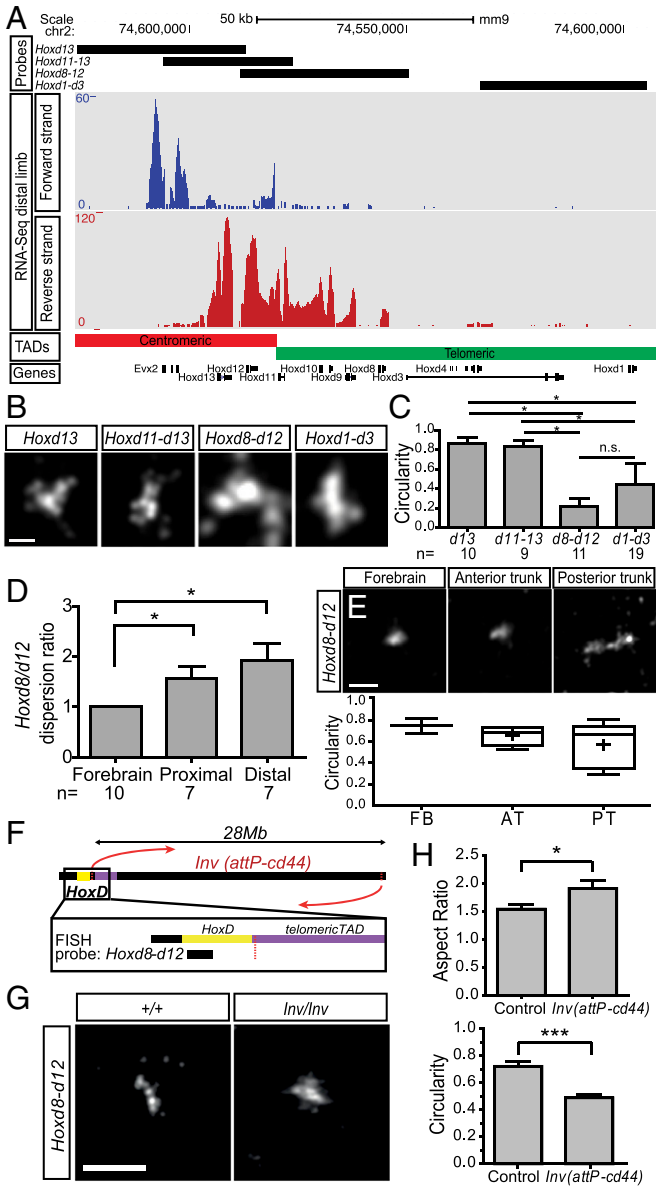

Fig. 3. STORM analysis using smaller probes in different control and mutant tissues. (*A*) RNA profile of distal forelimb cells showing the expression of *Hoxd8 to Hoxd13* (red) aligned with the positions of four fosmid probes (black, *Top*). The boundary between the centromeric (red) and telomeric (green) TADs is shown below, as well as the transcription of *Evx2* from the other DNA strand (blue). (*B*) STORM imaging using the four probes under *A* and their relative circularity index (*C*). (Scale bar, *B*, 100 nm.) (*D*) Refined analysis of the *Hoxd8* to *Hoxd12* probe in forebrain, proximal limb, and distal limb cells, quantifying the level of dispersion as depicted in *C* and *SI Appendix*, Fig. S2*B*. (Scale bar, 200 nm.) (*E*) STORM imaging of the *Hoxd8* to *Hoxd12* probe in E10.5 embryos in cells positioned along the anterior to posterior axis. AT, anterior trunk; FB, forebrain; PT, posterior trunk. (Scale bar, 200 nm.) (*F*) Scheme of the 28-Mb large *Inv(attP-cd44)* inversion (red arrows) removing the telomeric TAD (purple), and location of the *Hoxd8* to *Hoxd12* probe (black). (*G*) STORM imaging of the *Hoxd8* to *Hoxd12* region in E12.5 distal forelimb cells from either a homozygous *Inv(attP-cd44)* embryo (*Right*) or control littermate (*Left*). (Scale bar, 200 nm.) (*H*) Quantification of the aspect ratio and circularity in both configurations shown under *G*. $*P < 0.05$ and $***P < 0.001$, using Mann–Whitney *U* test. In *C* and *D*, $**P < 0.01$, using a Kruskall-Wallis test followed by Dunn's multiple comparison posttest. n.s., not significant.

was more pronounced and the circularity index lower, suggesting the telomeric gene desert may participate in the compaction of the system, rather than its elongation.

In this context, it is noteworthy that the part of the cluster displaying the highest level of decompaction was the *Hoxd8* to *Hoxd12* region, which precisely matches with the inter-TADs boundary (9, 16). This particular region of *HoxD*, located between genes strongly and constitutively interacting with either the centromeric (*Hoxd13*) or the telomeric (*Hoxd1, Hoxd4*) TADs, may thus display more flexibility, perhaps reflected by the capacity of *Hoxd8* or *Hoxd12* to switch their contacts from one TAD to the other in various limb cell-types (16). Interestingly, this region is strongly enriched in binding sites for architectural proteins such as CCCTC-binding factor (CTCF) and cohesin (41, 42), which are known for their capacity to organize genomic boundaries and domains, in particular at TAD boundaries (43). Whether the presence of several sites bound by CTCF in the sequence targeted by the *Hoxd8* to *Hoxd12* fosmid play a role in the elongation observed by STORM remains to be tested, however, as CTCF-driven interactions would be expected to increase compaction, rather than the opposite. An alternative explanation is that the resolution of our STORM approach, although allowing a clear distinction between fully compacted and decompacted *Hox* clusters, may not easily detect mixed configurations, in particular when only a small part of the cluster differs in shape from the rest.

In conclusion, these data suggest the structural organization of the *HoxD* gene cluster may predate transcriptional activation and may subsequently be rather independent from its transcriptional status. Perhaps such an elongated structure is maintained in cells expressing subsets of *Hoxd* genes, whereas compaction occurs in those cells where genes are silent, such as the fetal brain. In this latter tissue indeed, an elongated structure was never observed. By using 2D and 3D FISH, it was previously reported that a decompaction of the *HoxD* cluster occurs in ES cells that are differentiating in vitro, and that this process is linked to the progressive reduction in levels of PRC1 components (22). With the resolution of our STORM approach, the *HoxD* cluster did not appear to adopt a compact structure, which would be released on differentiation. It is possible that the spatial architecture of a decondensed cluster differs only slightly between the active and inactive states, leading to the observation of a range of distances between localized probes used for FISH. The presence of polycomb complexes may, for instance, impose such distinct organizations of the *HoxD* cluster in space, while having little influence on its general level of compaction. In this context, a detailed analysis of these structures by super-resolution microscopy in ES cells mutant for components of either the PRC1 or PRC2 complexes may be informative.

Materials and Methods

All experiments involving animals were performed in agreement with the Swiss law on animal protection, with the appropriate legal authorizations to D.D. Tissues were isolated from E10.5 or E12.5 embryos, either wild-type or mutant for the Inv(*Nsi-Itga6*), Inv(*attP-cd44*), and Inv(*HoxD^{RVIII}-Cd44*) inversions (31). Mouse ES cells were grown in serum with 1,000 U/mL leukemia inhibitory factor under feeder-free conditions and G1-synchronized through mitotic shake off. 3D DNA FISH was as in ref. 5. Structured illumination images were acquired using a Nikon structured illumination microscopy setup (Eclipse T1 microscope fitted with a super-resolution Apochromat total internal reflection fluorescence 100×/ 1.49 NA objective IXON3 camera; Andor Technology). For STORM imaging, DNA FISH samples were imaged using a UPlanSApo 100×/1.40 oil objective (Olympus), and typically 10,000–15,000 snapshot images with a pixel size of 100 nm and an exposure time of 0.03 s were acquired to create one super-resolution (SR) image. SR images were reconstructed with the Octane software (44), and statistical differences between samples were evaluated with the Kruskall-Wallis test, followed by Dunn's multiple comparison posttest, with the exception of Fig. 3*H* (Mann–Whitney *U* test). RNA-Seq was performed according to the TruSeq Stranded Illumina protocol, with polyA selection. The reads were mapped to Ensembl Mouse assembly National Center for Biotechnology Information Mouse Assembly 37 (mm9) and translated into reads per gene (RPKM) using the Bioinformatics and Biostatistics Core Facility (BBCF), High-Throughput Sequencing station (available at htsstation.epfl.ch). An extended description of the materials, methods, and data analysis is provided in the *SI Appendix*.

ACKNOWLEDGMENTS. We thank the members of the D.D. laboratories for discussions and S. Boyle and W. Bickmore (Medical Research Council Edinburgh) for their help with setting up the FISH procedures. We also thank O. Burri and R. Guiet [Ecole Polytechnique Fédérale de Lausanne (EPFL)] for assistance with image analysis and T. Laroche for help with structured illumination microscopy, as well as B. Mascrez and S. Gitto for help with mutant stocks. We thank the Geneva Genomics Platform (University of Geneva) and the Bioinformatics and Biostatistics Core Facility (EPFL) in Lausanne for their assistance with RNA-Seq. This work was supported by funds from the EPFL, the University of Geneva, the Swiss National Research Fund, the European Research Council (ERC) Grant Systems*Hox*.ch, and the Claraz Foundation (to D.D.), as well as Swiss National Research Fund Grant CR33I2_149850 and ERC Grant PALMassembly (to S.M.).

1. Bickmore WA, van Steensel B (2013) Genome architecture: Domain organization of interphase chromosomes. *Cell* 152(6):1270–1284.
2. de Laat W, Duboule D (2013) Topology of mammalian developmental enhancers and their regulatory landscapes. *Nature* 502(7472):499–506.
3. Gorkin DU, Leung D, Ren B (2014) The 3D genome in transcriptional regulation and pluripotency. *Cell Stem Cell* 14(6):762–775.
4. Chambeyron S, Bickmore WA (2004) Does looping and clustering in the nucleus regulate gene expression? *Curr Opin Cell Biol* 16(3):256–262.
5. Morey C, Da Silva NR, Perry P, Bickmore WA (2007) Nuclear reorganisation and chromatin decondensation are conserved, but distinct, mechanisms linked to Hox gene activation. *Development* 134(5):909–919.
6. van de Corput MP, et al. (2012) Super-resolution imaging reveals three-dimensional folding dynamics of the β-globin locus upon gene activation. *J Cell Sci* 125(Pt 19): 4630–4639.
7. de Laat W, Dekker J (2012) 3C-based technologies to study the shape of the genome. *Methods* 58(3):189–191.
8. Montavon T, et al. (2011) A regulatory archipelago controls Hox genes transcription in digits. *Cell* 147(5):1132–1145.
9. Dixon JR, et al. (2012) Topological domains in mammalian genomes identified by analysis of chromatin interactions. *Nature* 485(7398):376–380.
10. Nora EP, et al. (2012) Spatial partitioning of the regulatory landscape of the X-inactivation centre. *Nature* 485(7398):381–385.
11. Nora EP, Dekker J, Heard E (2013) Segmental folding of chromosomes: A basis for structural and regulatory chromosomal neighborhoods? *BioEssays* 35(9):818–828.
12. Schwarzer W, Spitz F (2014) The architecture of gene expression: Integrating dispersed cis-regulatory modules into coherent regulatory domains. *Curr Opin Genet Dev* 27:74–82.
13. Lonfat N, Duboule D (April 23, 2015) Structure, function and evolution of topologically associating domains (TADs) at HOX loci. *FEBS Lett*, 10.1016/j.febslet.2015.04.024.
14. Woltering JM, Noordermeer D, Leleu M, Duboule D (2014) Conservation and divergence of regulatory strategies at Hox Loci and the origin of tetrapod digits. *PLoS Biol* 12(1):e1001773.
15. Berlivet S, et al. (2013) Clustering of tissue-specific sub-TADs accompanies the regulation of HoxA genes in developing limbs. *PLoS Genet* 9(12):e1004018.
16. Andrey G, et al. (2013) A switch between topological domains underlies HoxD genes collinearity in mouse limbs. *Science* 340(6137):1234167.
17. Lonfat N, Montavon T, Darbellay F, Gitto S, Duboule D (2014) Convergent evolution of complex regulatory landscapes and pleiotropy at Hox loci. *Science* 346(6212):1004–1006.
18. Montavon T, Duboule D (2013) Chromatin organization and global regulation of Hox gene clusters. *Philos Trans R Soc Lond B Biol Sci* 368(1620):20120367.
19. Delpretti S, et al. (2013) Multiple enhancers regulate Hoxd genes and the Hotdog LncRNA during cecum budding. *Cell Reports* 5(1):137–150.
20. Giorgetti L, et al. (2014) Predictive polymer modeling reveals coupled fluctuations in chromosome conformation and transcription. *Cell* 157(4):950–963.
21. Williamson I, et al. (2014) Spatial genome organization: Contrasting views from chromosome conformation capture and fluorescence in situ hybridization. *Genes Dev* 28(24):2778–2791.
22. Eskeland R, et al. (2010) Ring1B compacts chromatin structure and represses gene expression independent of histone ubiquitination. *Mol Cell* 38(3):452–464.
23. Noordermeer D, et al. (2011) The dynamic architecture of Hox gene clusters. *Science* 334(6053):222–225.
24. Manley S, Gunzenhäuser J, Olivier N (2011) A starter kit for point-localization super-resolution imaging. *Curr Opin Chem Biol* 15(6):813–821.
25. Huang B, Wang W, Bates M, Zhuang X (2008) Three-dimensional super-resolution imaging by stochastic optical reconstruction microscopy. *Science* 319(5864):810–813.
26. Benke A, Manley S (2012) Live-cell dSTORM of cellular DNA based on direct DNA labeling. *ChemBioChem* 13(2):298–301.
27. Montavon T, Le Garrec J-F, Kerszberg M, Duboule D (2008) Modeling Hox gene regulation in digits: Reverse collinearity and the molecular origin of thumbness. *Genes Dev* 22(3):346–359.
28. Bernstein BE, et al. (2006) A bivalent chromatin structure marks key developmental genes in embryonic stem cells. *Cell* 125(2):315–326.
29. Papageorgiou S (2006) Pulling forces acting on Hox gene clusters cause expression collinearity. *Int J Dev Biol* 50(2-3):301–308.
30. Soshnikova N, Duboule D (2009) Epigenetic temporal control of mouse Hox genes in vivo. *Science* 324(5932):1320–1323.
31. Spitz F, Herkenne C, Morris MA, Duboule D (2005) Inversion-induced disruption of the Hoxd cluster leads to the partition of regulatory landscapes. *Nat Genet* 37(8):889–893.
32. Tschopp P, Duboule D (2014) The genetics of murine Hox loci: TAMERE, STRING, and PANTHERE to engineer chromosome variants. *Methods Mol Biol* 1196:89–102.
33. Tschopp P, Duboule D (2011) A regulatory 'landscape effect' over the HoxD cluster. *Dev Biol* 351(2):288–296.
34. Bickmore WA (2013) The spatial organization of the human genome. *Annu Rev Genomics Hum Genet* 14:67–84.
35. Noordermeer D, et al. (2014) Temporal dynamics and developmental memory of 3D chromatin architecture at Hox gene loci. *eLife* 3:e02557.
36. Marks H, et al. (2012) The transcriptional and epigenomic foundations of ground state pluripotency. *Cell* 149(3):590–604.
37. Phillips-Cremins JE, et al. (2013) Architectural protein subclasses shape 3D organization of genomes during lineage commitment. *Cell* 153(6):1281–1295.
38. Ferraiuolo MA, et al. (2010) The three-dimensional architecture of Hox cluster silencing. *Nucleic Acids Res* 38(21):7472–7484.
39. Song F, et al. (2014) Cryo-EM study of the chromatin fiber reveals a double helix twisted by tetranucleosomal units. *Science* 344(6182):376–380.
40. Zhang B, Wolynes PG (2015) Topology, structures, and energy landscapes of human chromosomes. *Proc Natl Acad Sci USA* 112(19):6062–6067.
41. Soshnikova N, Montavon T, Leleu M, Galjart N, Duboule D (2010) Functional analysis of CTCF during mammalian limb development. *Dev Cell* 19(6):819–830.
42. Gómez-Díaz E, Corces VG (2014) Architectural proteins: Regulators of 3D genome organization in cell fate. *Trends Cell Biol* 24(11):703–711.
43. Van Bortle K, et al. (2014) Insulator function and topological domain border strength scale with architectural protein occupancy. *Genome Biol* 15(6):R82.
44. Niu L, Yu J (2008) Investigating intracellular dynamics of FtsZ cytoskeleton with photoactivation single-molecule tracking. *Biophys J* 95(4):2009–2016.